Inorganic Chemistry

Article

pubs.acs.org/IC

Efficient Fluorinating Agent through Topochemical Fluorination of Co–Fe Layered Double Hydroxides

Nicolas Louvain,*[,†] Jérémy Peyroux, Marc Dubois, Wikenson Simond, and Fabrice Leroux

Clermont Université, Université Blaise Pascal, Institut de Chimie de Clermont-Ferrand, BP 10448, F-63000 Clermont-Ferrand, France

CNRS, UMR 6296, Institut de Chimie de Clermont-Ferrand, F-63177 Aubière, France

Supporting Information

ABSTRACT: Mixed-metal inorganic fluoride, $Co_{0.60}Fe_{0.40}F_3$, solid solutions are obtained through topochemical reactions of $Co_2FeCl(OH)_6{\cdot}2H_2O$ LDH with molecular fluorine, F_2, at temperatures as low as 100 °C. This solid solution possesses interesting $F^\bullet$-releasing ability, and its efficiency as a solid-state fluorinating agent is demonstrated on a commercial polyethylene film. ^{19}F solid state NMR and contact angle measurements underline the efficient fluorination of this polymer.

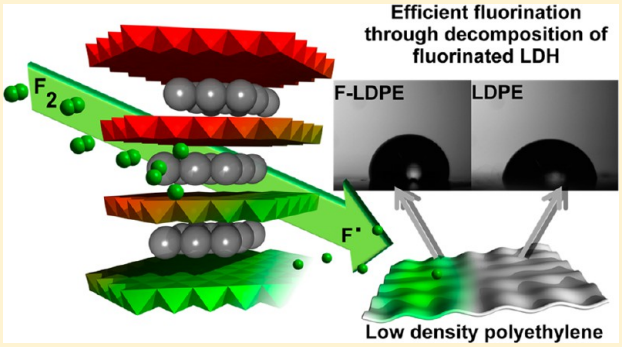

INTRODUCTION

In the fields of pharmacology, agrochemicals, and functionalized materials, fully or partially fluorinated compounds exhibit unique chemical, biological, and physical properties. Selective introduction of fluorine atoms into organic molecules or carbonaceous materials allows reaching the targeted biological, tribological, or electrochemical required properties.[1−3] Selectivity of the fluorination may be achieved thanks to a specific fluorinating agent (FA). The panel of solid FAs is rather large: transition-metal fluorides, ReF_7, ReF_6, OsF_6, IrF_6, UF_6, RuF_5, VF_5, and CrF_5, and transition-metal oxide fluorides, VOF_3, $MoOF_4$, WOF_4, $ReOF_4$, $ReOF_5$, OsO_3F_2, OsO_2F_3, $OsOF_5$, and $OsOF_4$. The oxidation state and coordination geometry of the FA act on the selectivity of the reaction with organic compounds. For examples, in the reaction of CH_2Cl_2 with ReF_6, 85% of available fluorine is used to yield CH_2ClF, whereas, with UF_6, all of the available fluorine is utilized to give $CHCl_2F$.[4] Titanium tetrafluoride can efficiently be used for stereoselective synthesis of 4-fluorotetrahydropyran via Prins cyclization in good yields.[5] Solid FAs are more versatile reagents than molecular fluorine, and the example of the fluorination of fullerenes is well representative of their efficiency. Unlike direct fluorination, which gives mainly a broad and continuous distribution of the species with fluorine content centered between $C_{60}F_{36}$ and $C_{60}F_{48}$, compounds having specific compositions $C_{60}F_x$, x = 2, 16, 18, 20, or 36, were prepared and isolated with binary metal fluorides (AgF, AgF_2, MnF_3, CoF_3, CeF_4, or TbF_4), some complex salts (K_2PtF_6 or K_3CoF_6), and a MnF_3–KF mixture. Fluorination degree of fullerene is mainly thermodynamically controlled.[6] Because of different diffusion and reactivity into or with carbonaceous (nano)materials,[7−9] carbides,[10] or polymers,[11,12] the fluorination mechanisms differ for molecular (F_2) and atomic fluorine ($F^\bullet$), the latter being released by the thermal decomposition of the FA.

Our study focuses on the synthesis of new fluorinating agents containing Co and Fe elements. CoF_3 and FeF_3 are intrinsically potential FAs according to the following reaction $MF_3 \rightarrow MF_2 + F^\bullet$. The standard formation enthalpies $\Delta_f H^\circ_{298}$ are equal to 199 and 356 kJ mol^{-1} for CoF_3 and FeF_3, respectively, higher than the ones for TbF_4 (168 kJ mol^{-1}), known as an excellent FA, and F_2 (79 kJ mol^{-1}).[6] This results in higher decomposition temperatures and higher reaction temperatures to fluorinate the sample. Indeed a mixture of Co^{3+} and Fe^{3+} ions may destabilize each of them in comparison with the single fluorides and finally decrease the decomposition temperature. Therefore, an enticing and elegant approach consists in destabilizing both fluorides through a solid solution between Co and Fe to yield an intimate mixed cation fluoride $Co_xFe_{1-x}F_3$. This requires from such pristine structure to present a relatively well-ordered arrangement between the metallic ions at the atomic scale in association with its appropriate reactivity. This is reminiscent of topochemical reaction occurring during reduction or other reactions (dehydration, chlorination) involving reactive sites and rapid reaction diffusion because of large reactivity or interface.[13] The FA candidate should then possess an open structure (large edge-surface), an appropriate relative metal composition, and sites reactive toward fluorination at low temperatures. For such

Received: August 27, 2013
Published: December 23, 2013

   dx.doi.org/10.1021/ic402193x | Inorg. Chem. 2014, 53, 852–860

aim, layered double hydroxides (LDHs) were used as precursors of the fluorination with molecular F_2 gas. LDHs, well-known as hydrotalcite-like compounds or anionic clays, are a large class of natural and synthetic materials that have a general formula $M^{II}_{1-x}M^{III}_x(OH)_2(A_n^-)_{x/n}\cdot mH_2O$.[14] Isomorphous replacement of some M^{II} (Co^{2+} in our study) cations by M^{III} (Fe^{3+}) ones produces layers with a positive charge, which is compensated by anions located, along with water molecules, in the interlayer galleries,[15] having in mind that multiple substitutions on the octahedral $M(OH)_6$ sites are possible.[16,17] The Co/Fe ratio can be tuned through the synthesis conditions of the LDH,[18,19] which is then fluorinated keeping the initial Fe−Co distribution mostly intact but evidently not the pristine lamellar structure. The first part of the paper will be devoted to the fluorination of the selected LDHs in order to define the experimental conditions to convert hydroxide groups into fluorides. Even if the LDH has extensively been considered as precursor to yield mixed-cation oxides for catalysis,[14,20] such conversion was never investigated to the best of our knowledge. Then, after the characterization of the resulting fluorinated samples, the last part will focus on the use of the as-obtained fluorinated LDH as FA to covalently graft fluorine atoms onto the surface of a commercial polymer, polyethylene, keeping in mind that the fluorination process is efficient to functionalize polymers with resulting enhanced hydrophobicity and chemical stability, gas barrier properties, antibacterial properties, printability, and low friction coefficients.[21]

EXPERIMENTAL DETAILS

$Co_2FeCl(OH)_6\cdot 2H_2O$ Synthesis. Hydrated metal chlorides and sodium hydroxide were used as supplied by Aldrich, without further purification. Solutions of the reactants were added to the reactor with peristaltic pumps. The hydrotalcite-like material $Co_2FeCl(OH)_6\cdot 2H_2O$ was prepared via the conventional coprecipitation method, and the resulting LDH phase was then used as precursor for the fluorination. Experimentally, 100 mL of a solution of the $CoCl_2$ (13.706 g, 5.76 mmol) and $FeCl_3$ (7.785 g, 2.88 mmol) hydrated salts with a Co^{II}/Fe^{III} ratio of 2 was added dropwise to distilled water under a nitrogen atmosphere, to avoid the carbonate contamination from air. The solution of salts was added at a constant flow of 2.0 mL min^{-1} for 3 h. The pH was kept constant at a value of 9 ± 0.1 through the addition of a sodium hydroxide solution. After a 3 h aging, the slurries were centrifuged and finally washed several times with distilled water.

LDH Fluorination. LDH powder samples were fluorinated under a gaseous flow of molecular fluorine at temperatures up to 400 °C. Pure F_2 gas was used (Solvay Fluor and Derivate, purity 98−99% (v/v) with HF max 0.5% (v/v) and other gases, primarily O_2/N_2, at approximately 1.0% (v/v)). The direct F_2-gas fluorination process was performed in dedicated fluorine equipment using special handling procedures. A cylindrical passivated nickel reactor of approximately 50 cm in length and offering a volume of approximately 1 L was used for the reaction. The heating was ensured by a horizontal tubular oven surrounding the reactor, with a domain of homogeneous temperature of approximately 10 cm. All samples were set in a passivated nickel boat. The passivation consists in a homogeneous coating of NiF_2, which is formed under F_2 gas at 500 °C prior to the experiments. A typical one-shot fluorination procedure can be described as follows: approximately 250 mg of LDH powder was placed on a passivated nickel boat, and the powder surface exposed to the reactive atmosphere was manually limited to 2−4 cm^2, which induced a thickness of the powdered deposit of a few millimeters. The boat was placed at the center of the fluorination oven, which was flushed for 2 h with nitrogen while the temperature was increased to 100 °C (heating rate of 10 °C min^{-1}). This step ensures the removal of adsorbed water molecules, which may react with F_2 to form HF, which may act as catalyst, thus resulting in inhomogeneous fluorination. After the oven cooled to room temperature, fluorine was introduced, and the temperature was set to the desired one. After 15 h, fluorine flow was stopped, and the reactor oven was flushed with nitrogen until the system cooled to room temperature. The product was finally transferred to a dry glovebox with humidity level below 0.05 ppm (yield 90−95% on the basis of the formulation $Co_{0.60}Fe_{0.40}F_3$ as derived from X-ray diffraction (XRD) and thermogravimetric (TG) measurements).

Fluorinated LDHs as Fluorinating Agents. To validate the use of fluorinated LDHs as efficient FAs, fluorination with $Co_{0.60}Fe_{0.40}F_3$ (280 mg, 2 mmol) was performed on a low density polyethylene (LDPE) film surface in a double-compartment nickel reactor. When $Co_{0.60}Fe_{0.40}F_3$ is heated to 400 °C, it decomposes according to the reaction (supported by XRD measurements, please refer to Supporting Information)

$$MF_3(s) \xrightarrow{\Delta} MF_2(s) + F^{\bullet}$$

In the first compartment, $Co_{0.60}Fe_{0.40}F_3$ (280 mg, 2 mmol) was placed in an alumina boat. In the cold end of the reactor (externally cooled by water flow), LDPE was placed in a passivated nickel boat. The reactor was then evacuated for 2 h and isolated. The first compartment was subsequently heated to 400 °C for 15 h. Once at room temperature, the reactor oven was flushed with nitrogen gas. Approximately 30 mg of fluorinated LDHs was consumed in the global process.

LDPE Direct Fluorination. For comparison, LDPE films were fluorinated under a mixed gaseous flow of nitrogen and molecular fluorine at room temperature in a cylindrical nickel reactor. Pure F_2 gas was used (Solvay Fluor and Derivate, purity 98−99% (v/v) with HF max 0.5% (v/v) and other gases, primarily O_2/N_2, at approximately 1.0% (v/v)). The total pressure of gases used in fluorination experiments was fixed at 1013 mbar. In a typical experiment, polymer samples (180−200 cm^2) were set on a dedicated cylindrical passivated nickel boat and placed at the center of the fluorination oven, which was flushed for 1 h with nitrogen gas. Each sample was then submitted to a reactive N_2/F_2 1:1 gaseous flow for 1 to 280 min. The fluorine flow was subsequently stopped, and the reactor oven was flushed with nitrogen for 1 h. Fluorinated LDPE polymers were finally transferred to dry storage bags for analyses. Prior to the fluorination, primary vacuum (10^{-2} mbar) was performed into the reactor. Polymer samples were placed in the second compartment, which was cooled from outside by water, so the temperature of a polymer was close to room temperature. During the fluorination, the pressure continuously increased because of both the decomposition of the fluorinating agent and the increase of the temperature. When FA was heated without polymer, the pressure reached a value of 20 mbar after 24 h (2 mmol of $Co_{0.60}Fe_{0.40}F_3$); such a value is not obtained when the polymer is present in the reactor because of the fluorination and the consumption of fluorine. The final pressure is lower than in the case of the direct process using F_2 gas (1013 mbar). The fluorination duration using F_2 was selected (shorter treatment) in order to take into account this difference and to obtain similar fluorine content.

Solid-State Characterizations. X-ray powder diffraction (XRPD) experiments were carried out on a PANalytical X-Pert Pro diffractometer equipped with a diffracted beam monochromator Cu Kα source and an X'celerator linear detector. The counting time was 10 s, and the angle step was 0.08°. Thermogravimetric analysis was performed under inert argon gas on a Shimadzu TGA-50 thermogravimetric analyzer instrument from 25 to 600 °C with a heating ramp of 10 °C·min^{-1}. Infrared spectroscopy (ATR mode) was measured on freshly prepared samples stored under argon on an FTIR spectrometer NICOLET 5700 (Thermo Electron).

Scanning electronic microscopy (SEM) was carried out on an ultrahigh resolution Supra 55VP field-effect scanning electron microscope equipped with a Gemini column and high efficiency in-lens secondary electron detector. The instrument was fitted with an Oxford Instruments X-Max large area detector for analytical energy-dispersive X-ray spectroscopy (using the INCA 350 software).

dx.doi.org/10.1021/ic402193x | Inorg. Chem. 2014, 53, 852−860

For pair distribution function (PDF) analysis, the powdered F-LDH-150 and references CoF_3 and FeF_3 were packed in a Kapton capillary and sealed to prevent exposure to air. PDF analyses were carried out based on X-ray scattering data measured at the 11-ID-B beamline at the Advanced Photon Source at Argonne National Laboratory. High energy X-rays (λ = 0.2128 Å) were used in combination with a large amorphous silicon based area detector to collect data to high values of momentum transfer $Q \approx 22$ Å^{-1}.[22,23] Diffraction images were integrated within fit2D to obtain the one-dimensional diffraction data.[24] PDFs, $G(r)$, were extracted from the data within pdfgetX2[25] after correcting for background and Compton scattering.

Fluorinated LDPE Characterizations. ^{19}F NMR experiments were realized with a Bruker Avance spectrometer with Larmor frequency of 282.2 MHz. A magic angle spinning probe operating with 2.5 mm rotors were used for 34 kHz spinning rates. For ^{19}F MAS spectra, a simple sequence was used with a single $\pi/2$ pulse duration of 4.0 μs. ^{19}F chemical shifts were externally referenced to CF_3COOH and were referenced with accord to $CFCl_3$ (δCF_3COOH = −76.55 ppm vs $\delta CFCl_3$).

Static contact angles were measured using the conventional Owens−Wendt method on an Attension Theta Lite optical tensiometer with an imaging source camera. All contact angles are the mean value of different measurements performed on four different locations on the sample's surface. Two different liquids were used, distilled water and formamide.

RESULTS AND DISCUSSION

LDHs Fluorination. The XRD patterns of the LDH precursor and LDH fluorinated at 50, 100, 150, 200, and 400 °C, denoted F-LDH-50, F-LDH-100, F-LDH-150, F-LDH-200, and F-LDH-400, respectively, are shown in Figure 1. The XRD

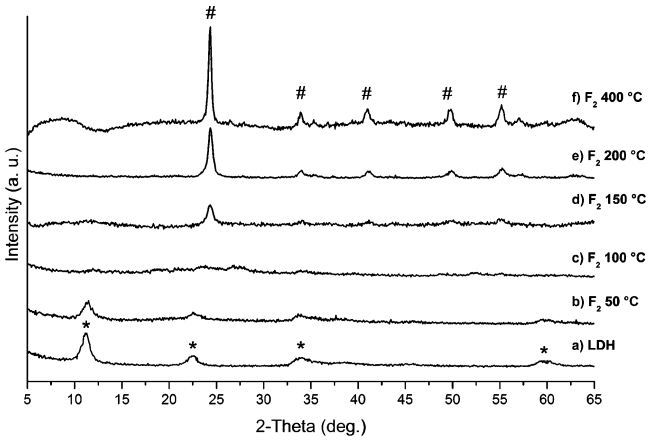

Figure 1. XRD patterns of pristine and fluorinated LDH precursors; * and # mark the presence of LDH and rhombohedral FeF_3 structures, respectively.

of the LDH precursor presents features consistent with the common layered structure of LDH materials, which is usually described with a hexagonal lattice using rhombohedral symmetry with only $-h + k + l = 3n$ reflections. The peaks at 2θ = 11.2°, 22.4°, 33.8°, 38.7°, 45.8°, and 59.8° correspond to (003), (006), (102), (015), (018), and (110) *hkl* planes, respectively (Figure 1a). The coherence length along the stacking direction was estimated from the full width at half minimum of the (006) reflection using the Scherrer equation and found to be equal to 71.5 nm, which corresponds to roughly ⟨fwhm/d⟩ stacked platelets. The LDH precursor submitted to F_2 fluorination at 50 °C, F-LDH-50, does not display any structural change (Figure 1b) but presents a reduced crystallinity (coherence length of 56.5 nm) that indicates the beginning of an amorphization, peeling off LDH sheets, and at the same time local in-plane disordering since the (110) diffraction peak decreases in intensity. When fluorinated at 100 °C, the product is amorphous and characteristic peaks from the hydrotalcite-like materials have disappeared. Higher fluorination temperatures lead to the appearance of a new crystalline phase with a main peak centered on 2θ = 24.35°. At 200 °C and higher, XRD patterns are typical of a distorted ReO_3-type structure, which is also best described as an A-site deficient rhombohedral-type perovskite (space group $R\bar{3}c$), adopted by most $M^{III}F_3$ inorganic fluorides (M^{III} = Fe, Co, Ti, etc.).[26] Although the LDH precursor is composed of Co^{II} and Fe^{III}, no crystallized $Co^{II}F_2$ is obtained because of the highly oxidant character of gaseous molecular fluorine, thus giving immediate rise to $Co^{III}F_3$ or $Fe^{III}F_3$. Assuming the structure to be correct (i.e., M^{III} = Fe or Co), peaks at 2θ = 24.35°, 33.87°, 40.98°, 49.75°, and 55.18° may correspond to (011), (211), (−101), (102), (022), and (123) *hkl* planes of the distorted ReO_3-type structure. Having this in mind and taking into account that the most intense reflection is the (011), the fluorination of LDH at 150 °C unambiguously produces $M^{III}F_3$ (M = Fe or Co) as the main, yet poorly, crystallized phase, as shown by the presence of the peak centered on 24.35°, which may correspond to the (011) *hkl* plane. The evolution of the crystallinity of the fluorinated materials is also directly observed from the SEM images. Figure 2a reveals LDH clusters of rather

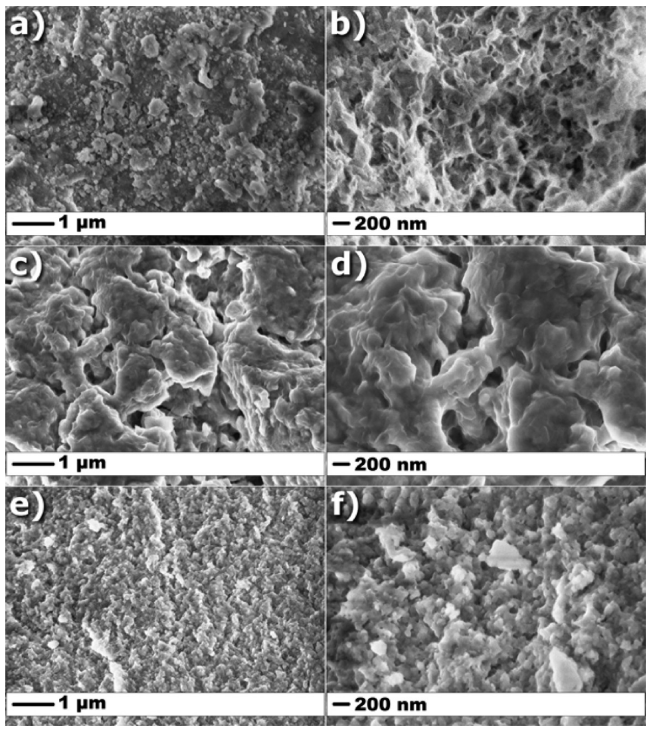

Figure 2. SEM images of pristine LDH (a, b), F-LDH-100 (c, d), and F-LDH-200 (e, f).

ill-defined morphology with various sizes from 200 to more than 500 nm. These large clusters are composed of small aggregates in which the typical LDH layered-like growth could faintly be discerned only (Figure 2b); the stacking thickness could be estimated to be smaller than 100 nm, a result in accordance with the value obtained from the XRD pattern.

dx.doi.org/10.1021/ic402193x | Inorg. Chem. 2014, 53, 852−860

After a 100 °C fluorination, the initial cluster morphology is completely lost, and Figure 2c shows fritted aggregates of approximately 1 μm, made up of many smaller fused particles (Figure 2d), characteristic of amorphous materials, thus confirming the diffraction data (Figure 1c). Figure 2e,f shows SEM images of the LDH precursor fluorinated at 200 °C and reveals sponge-like aggregates, formed of self-assembled nanoparticles of about 200 nm in size (Figure 2f). Fluorination at 200 and 400 °C results in crystallized fluorides (Figures 1e,f).

The influence of the fluorination temperature has been investigated through FT-IR spectroscopy (Figure 3a). As shown by the XRD study, the fluorination at 50 °C does not lead to a clear interaction of fluorine with the LDH matrix, and the spectrum is quite similar to the LDH precursor one. On the other hand, the product from the fluorination at 100 °C presents some broad signal typical of the M−F (M = metal) stretching in the 650−250 cm^{-1} region. This signal clearly appears on the spectrum of the product of the 200 °C fluorination with two broad bands (500 and 360 cm^{-1}) and one weak band at 260 cm^{-1}. The FTIR spectra allow us to conclude that the ignition of reactivity of fluorine toward LDH material starts at 100 °C, in good accordance with the previous XRD study. According to the initial composition of the LDH, $Co^{II}_2Fe^{III}Cl(OH)_6{\cdot}2H_2O$, two possibilities could be encountered: either a heterogeneous mixture of CoF_3 and FeF_3 phases or a homogeneous mixed-metal phase $Co_xFe_{1-x}F_3$ (i.e., a solid solution). To formulate an answer to the previous question, the far-infrared spectrum of the LDH fluorinated at 200 °C is compared with the spectra of the pure CoF_3 and FeF_3 phases (please refer to Supporting Information for detailed synthesis), as displayed in Figure 3b. The experimental signal (Figure 3b, F_2 200 °C) is significantly different from both spectra of the pure phases but shares similar features with the weighted sum of CoF_3 and FeF_3 spectra, such as broad peaks red-shifted of 5−10 cm^{-1}. Thus, the fluorinated LDH materials may be composed of IR vibration signature representative of both CoF_3 and FeF_3 phases.

In order to further investigate the composition of the fluorinated LDH materials, whether the phase is a mixture of phases or a solid, Rietveld refinements were conducted on the product fluorinated at 200 and 400 °C (Figure 4a and Supporting Information). For the former one, lattice parameters are calculated to be a_{hex} = 5.1017(23) Å and c_{hex} = 13.2239(74) Å, which are similar to previous reports on FeF_3 but significantly different, and this may be the signature of the existence of a Co/Fe solid solution. To check this assumption, pure CoF_3 and FeF_3 phases were also analyzed by XRD, and their structural parameters were refined. The results are listed in Table 1. All structures were refined in the rhombohedral $R\bar{3}c$ space group. Figure 4b shows the variation of cell parameters *a*

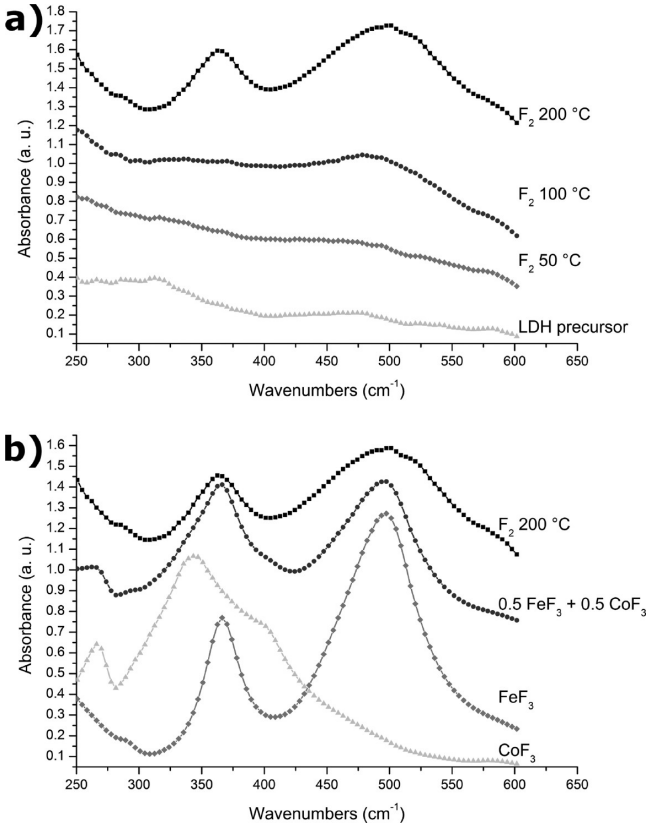

Figure 3. Far IR spectra of pristine and fluorinated LDH precursors (a); far IR spectra of pure CoF_3 and FeF_3, and F-LDH-200 compared with its simulated spectrum (b).

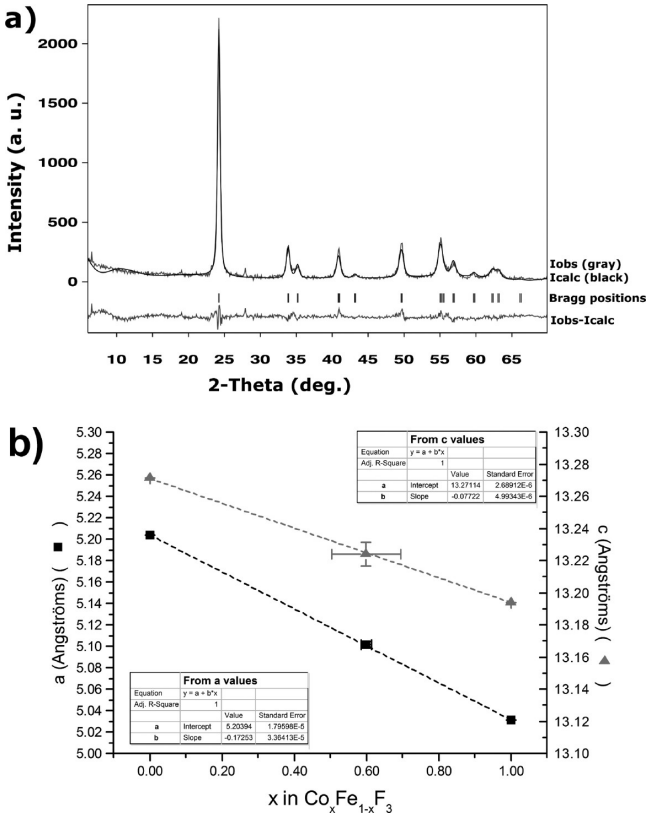

Figure 4. Rietveld refinement XRD pattern of F-LDH-200 (a) and cell parameters of CoF_3, FeF_3, and F-LDH-200 as derived from Rietveld refinement, showing the plot of Vegar's law (b).

Table 1. Cell Parameters of FeF_3, CoF_3, and F-LDH-200 as Derived from Rietveld Refinement

	a (Å)	*c* (Å)
FeF_3	5.2039(4)	13.2711(4)
F-LDH-200	5.1017(23)	13.2239(74)
CoF_3	5.0314(1)	13.1939(2)

dx.doi.org/10.1021/ic402193x | *Inorg. Chem.* 2014, 53, 852−860

and c, assuming a theoretical solid solution $Co_xFe_{1-x}F_3$ from $x = 0$ to $x = 1$. According to Vegar's law, the formula of F-LDH-200 can then be deduced from its refined parameters. The first important point to consider is the good agreement between the refined values of both a and c parameters and their expected values derived from Vegar's law (Figure 4b). When either a or c parameters are considered, calculations lead to an average value of x equal to 0.60 ($x = 0.59$ from a, and $x = 0.61$ from c; detailed results in Table S1, Supporting Information). Thus, the formula of the Co/Fe solid solution can be written as $Co_{0.60}Fe_{0.40}F_3$. From the formulation of the initial LDH precursor, an identical Co/Fe ratio should have led to $Co_{0.66}Fe_{0.33}F_3$ formula. The difference between the expected and observed Co/Fe ratio might come from the presence of Co^{3+} cations in an amorphous product, most probably CoX_3 (X = F or OH). Results obtained for F-LDH-400, the LDH phase fluorinated at 400 °C, show a slightly lower average Co^{3+} content in the formula (Figure S6, Table S2, Supporting Information) and this discrepancy might originate from the inception of the decomposition of the final fluorinated product, thus giving rise to an increased amount of amorphous Co^{3+}-based compound.

Obtaining a solid solution requires that the initial distribution of divalent and trivalent cations is maintained throughout the fluorination process without phase segregation, and this is possible only because molecular fluorine is highly reactive and reacts with the LDH precursor before its decomposition ($T \approx$ 250 °C). Demonstrated from the crystallized phases (fluorination temperature above 200 °C), the solid solution may be formed from 100 °C, according to IR data. In order to go further about F-LDH-150, its pair distribution function profile (PDF) was compared with those of CoF_3 and FeF_3 as references; the PDF profiles were obtained by Fourier transform of the data (Figure 5a), which correspond to a histogram of the interatomic distances. This technique allows the components of both the crystallized parts (diffracted intensities) and amorphous regions (diffused intensities) to be revealed. Figure 5b,c displays the patterns for CoF_3, FeF_3, and F-LDH-150. The intensities, related to the crystallinity, underline that F-LDH-150 is clearly amorphous. The comparison of the PDF profiles for FeF_3, CoF_3, and F-LDH-150 highlights different structures. F-LDH-150 seems to exhibit a phase of rutile MF_2-type, which could be an intermediate before the formation of ReO_3-type structure. Taking into account the interatomic distance corresponding to the first coordination spheres around Co and Fe atoms, F-LDH-150 exhibits a broad distribution located at higher distances than for the cases of CoF_3 and FeF_3. The differences may be explained by the presence of residual M−OH before the completion of the fluorination.

At this temperature, the completion of the "M−OH to MF" conversion might not be achieved. Thus, the thermal behavior of the fluorinated product has been investigated between 25 and 600 °C, and the results are presented in Figure 6. As for pure MF_3 compounds, the first thermal decomposition step should be the loss of mainly one fluorine atom (19 g mol^{-1}), according to the following equation,

$$Co_{0.60}Fe_{0.40}F_3 = Co_{0.60}Fe_{0.40}F_2 + F^{\bullet}$$

but also one residual OH (18 g mol^{-1}) in a dehydroxylation process (Figure S9, Supporting Information).

The LDH fluorinated at 100 °C decomposes in two steps at 140 and 200−250 °C and displays a weight loss of 16.2% at 400 °C, which corresponds to 0.97F/OH. This result is in good accordance with the reactivity of fluorine with the precursor as emphasized by IR spectroscopy. According to the thermal behavior of the pure bulk phases, FeF_3 decomposes at 335 °C and CoF_3 at 440 °C (Figures S7 and S8, respectively, Supporting Information). Therefore, the two decomposition steps observed may correspond to the decomposition of the Fe−F and Co−F bonds at 140 and 200−250 °C, respectively, and the amorphous nature of the fluorinated product could be the reason for reduced thermal stability. The LDH fluorinated at 150 °C decomposes in a similar way, the two steps being at a slightly higher temperature (145 and 220−265 °C, respectively). The weight loss of 5.9% displayed at 200 °C corresponds to 0.36F, while the loss between 200 and 400

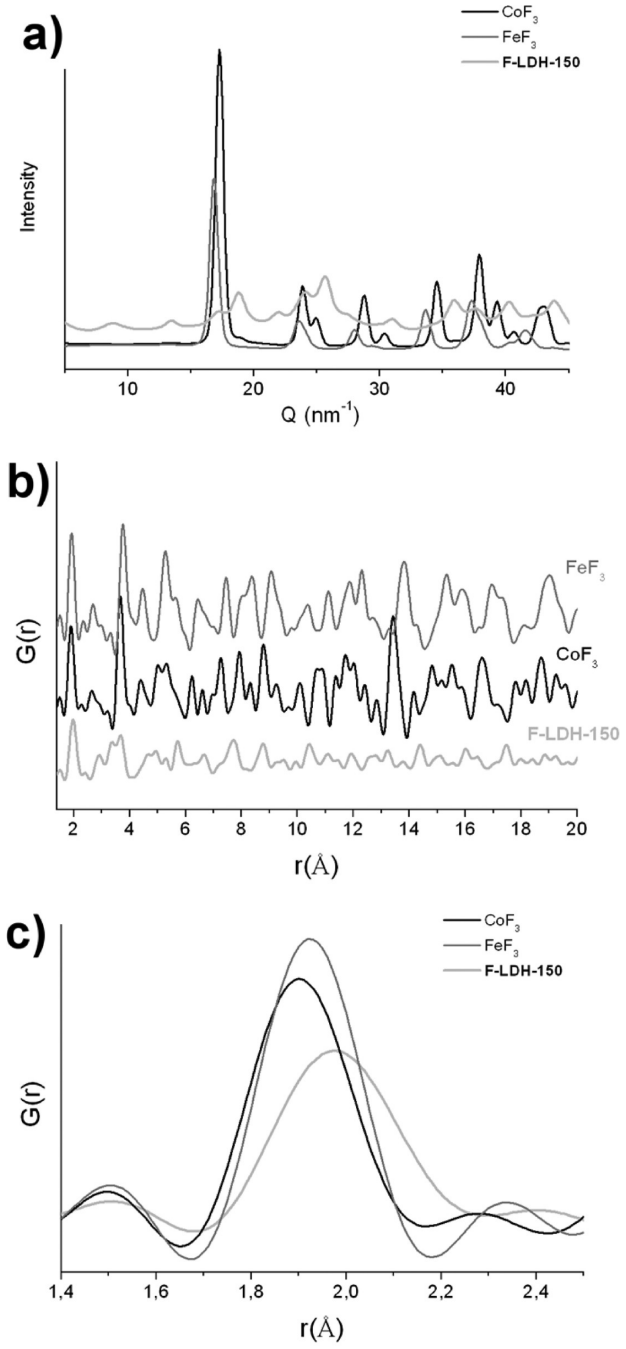

Figure 5. CoF_3, FeF_3, and F-LDH-150 PDF refinement results.

dx.doi.org/10.1021/ic402193x | Inorg. Chem. 2014, 53, 852−860

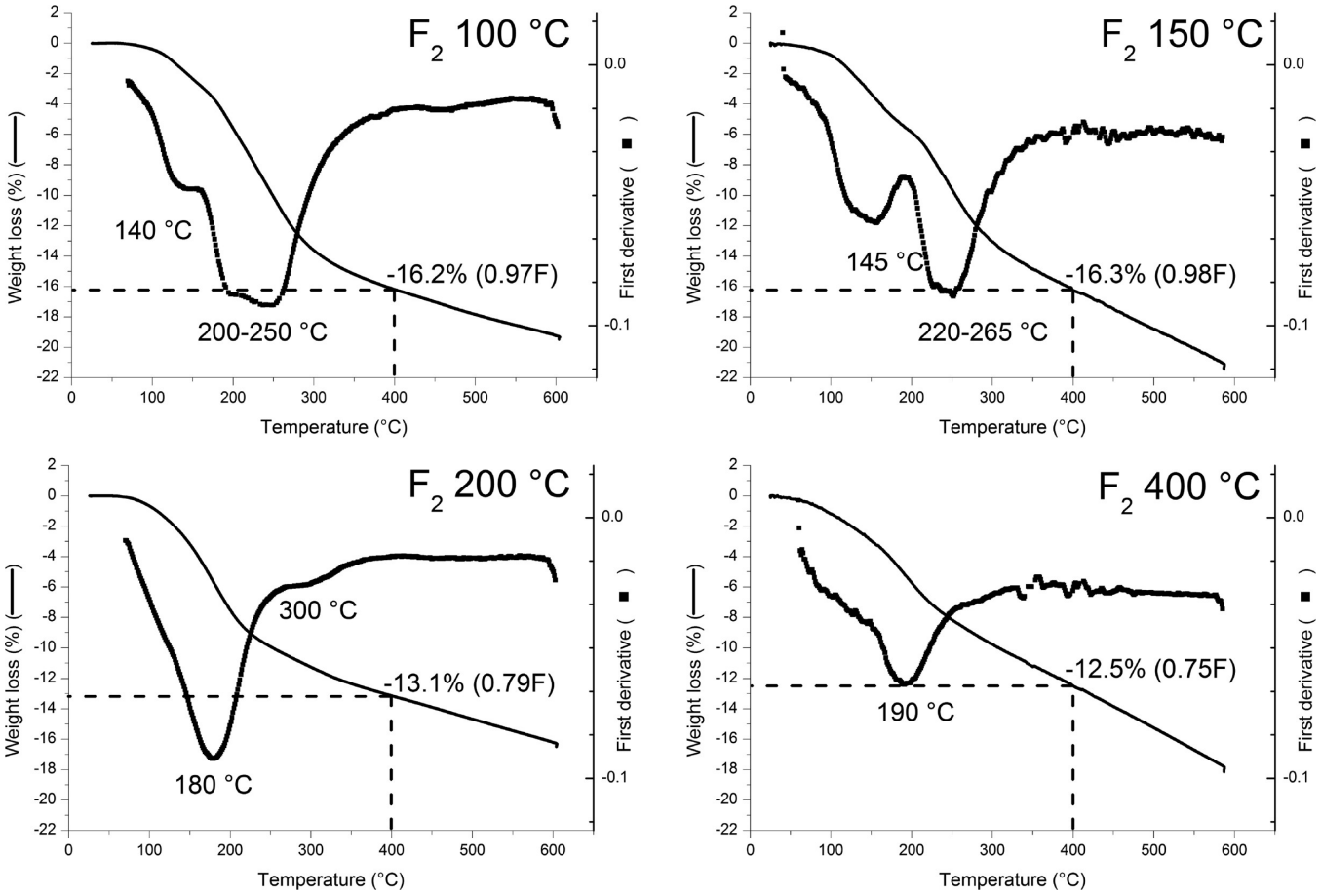

Figure 6. TG analyses of F-LDH-100, F-LDH-150, F-LDH-200, and F-LDH-400.

°C represents approximately 0.62F (with a global loss of 16.3% at 400 °C, that is, 0.98F), and thus the formula derived from the Rietveld analysis, $Co_{0.60}Fe_{0.40}F_3$, is confirmed by the TG results. After the fluorination at this temperature of 150 °C, the amount of the residual OH groups seems to be low taking into account the good accordance between TG and Rietveld analysis. For products obtained at higher temperatures, the decomposition of the fluorinated products occurs in one main step from 180 °C, thus underlining the homogeneous nature of the Co/Fe solid solution and the completion of the conversion from M−OH to MF. The thermal stability of the $Co_{0.60}Fe_{0.40}F_3$ matrix is further confirmed by smaller weight loss at 400 °C (13.1%, that is, 0.79F, and 12.5%, that is, 0.75F, for the products fluorinated at 200 and 400 °C, respectively) yet is weaker than that of the pure phases, FeF_3 and CoF_3, which display weight loss of only 3.22% (0.19F) and 2.87% (0.17F) at 400 °C (Figures S7 and S8, Supporting Information). F-LDH-150 is probably slightly destabilized in comparison with F-LDH-200 due to the presence of residual M−OH groups (140 versus 180 °C for the first weight loss for the cases of F-LDH-150 and F-LDH-200, respectively; Figure S10, Supporting Information).

Since a weaker thermal stability than that of the pure bulk phases corresponds to the ability to release atomic fluorine, the as-obtained fluorinated phase may serve as an efficient FA. The presence of residual OH groups is not excluded from our data. Their presence at the lowest fluorination temperature may favor the thermal defluorination by a decrease of the crystalline order of the solid solution $Co_{0.60}Fe_{0.40}F_3$.

F-LDH-150 was chosen for such aim because it corresponds to an intermediate state before the completion of the conversion (obtained for F-LDH-200) as underlined by FT-IR and XRD data. Successful fluorination of the target for F-LDH-150 would validate the concept for the highest fluorination temperature.

F-LDHs as Fluorinating Agents. The fluorinating ability of the fluorinated LDH materials has been estimated on a low density polyethylene (LDPE) film by using the LDH precursor submitted to F_2 at 150 °C (F-LDH-150) and compared with conventional direct fluorination with F_2 gas. For such aim, this latter process was optimized (duration, dilution of F_2 by N_2, gas flow rate) in order to reach close fluorine content estimated by weight uptake during the reaction (Table 2). The fluorinated films are denoted, according to their synthesis method, F-LDFE-F2 when submitted to molecular fluorine and F-LDPE-FA when solid state FA $Co_{0.60}Fe_{0.40}F_3$ was used. The F/C molar ratio of fluorinated LDPE (F-LDPE) was determined by weight uptake, and the results are presented in Table 2.

Table 2. Compositions Deduced by Weight Uptake of F-LDPE Synthesized by Controlled (F-LDH-150) and Direct (F_2) Methods at Room Temperature

sample	fluorination duration (min)	F/C (%)
LDPE (pristine)	0	0
F-LDPE-F2	5	0.08
F-LDPE-FA	900	0.05

dx.doi.org/10.1021/ic402193x | Inorg. Chem. 2014, 53, 852−860

FT-IR (ATR mode) spectra of F-LDPE films have been collected and are clearly different from the spectrum of pristine film (Figure 7a), as emphasized by the band appearing over the

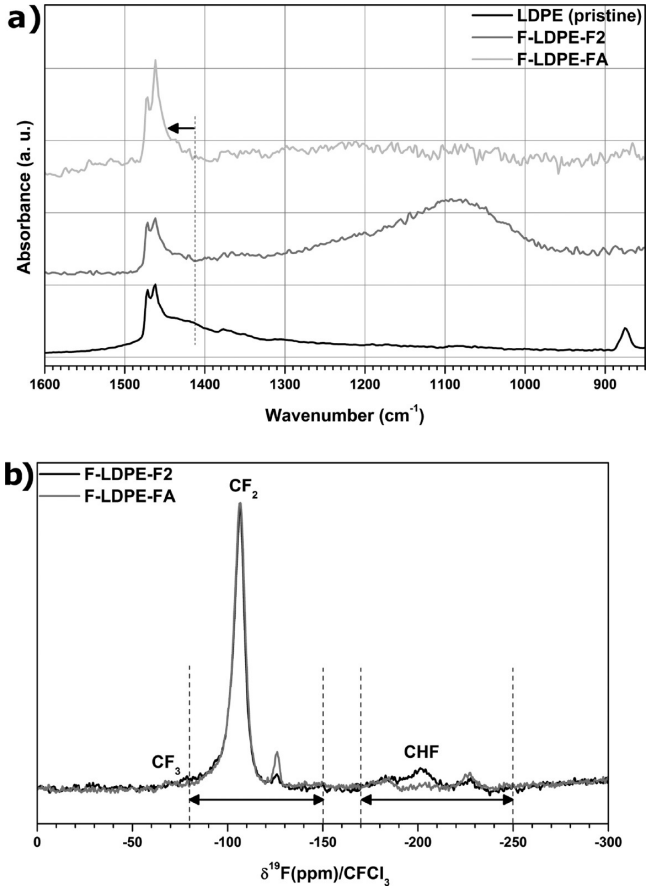

Figure 7. IR spectra of pristine and fluorinated LDPE polymer films (a); solid-state ^{19}F NMR spectra of fluorinated LDPE polymer films (b).

1400−800 cm^{-1} region, characteristic of C−F bonds vibration. Nevertheless, the band has a very low intensity in the spectra of F-LDPE-FA, as compared with F-LDPE-F2, and this might be due to the difference in reactivity between molecular fluorine F_2 and atomic fluorine $F^{\bullet}$. Their fluorination mechanisms are dissimilar as far as the diffusion is involved, and F_2 will interact mostly with the surface of the polymer while $F^{\bullet}$ may diffuse further in the polymer, thus resulting in a homogeneous fluorination throughout the volume of the polymer.[11] The ATR mode being mostly sensitive to the surface of the samples, the F-LDPE-F2 material shows a more pronounced C−F band than F-LDPE-FA, which does not rule out the presence of C−F bonds in the latter material. ^{19}F solid-state NMR experiments were then performed on F-LDPE films, and the results are shown in Figure 7b. The spectra exhibit bands with ^{19}F chemical shifts at approximately −200, −120, and −80 ppm, determined relative to $CFCl_3$ reference standard, which correspond to CF, CF_2, and CF_3 chemical groups, respectively.[27−31] In both case, in the operating conditions, the fluorination results preferentially in CF_2 groups, the amount of CHF being lower. The present experiments validate the presence of CF_x groups and the efficient transfer of fluorine from $Co_{0.60}Fe_{0.40}F_3$ as FA into the polymer.

Finally, contact angles were measured, and using the conventional Owens−Wendt method, surface energy (polar and dispersion components, total surface energy) was extracted.[32,33] Results are presented in Figure 8 and Table 3. It has been demonstrated that the total surface energy and its polar and dispersive components mainly depend on the type of fluorinating agent used.[34−41]

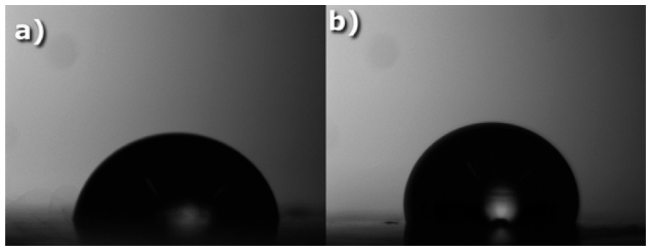

Figure 8. Contact angles of pristine (a) and LDPE polymer film fluorinated with F-LDH-150 FA (b).

Table 3. Total Surface Energy Parameters As Derived from Contact Angle Measurements with the Owens−Wendt Method

sample	θ_{water} (deg)	$\theta_{formamide}$ (deg)	polar component (mN m^{-1})	dispersion component (mN m^{-1})	total surface energy (mN m^{-1})
LDPE (pristine)	79.8	69.8	12.2	14.6	26.8
F-LDPE-F2	60.0	22.7	11.0	43.8	54.8
F-LDPE-FA	97.3	74.2	1.21	26.3	27.5

Although F-LDPE-F2 and F-LDPE-FA have similar fluorine content, the surface energy differs according to the fluorination route. The total surface energy of F-LDPE-FA is close to the energy obtained for the pristine sample but both polar and dispersive components change (Table 3). The drastic decrease of the polar component (from 12.2 to 1.21 mN m^{-1}, see Table 3) underlines the enhanced hydrophobicity of the polymer surface (Figure 8). This definitely validates the fluorination of the films through specific FAs with formation of characteristic fluorinated groups at the surface of the treated LDPE polymer.

Surprisingly, surfaces tend to be more hydrophilic after the direct fluorination treatment; the dispersive component changes from 14.6 to 43.8 mN m^{-1} (Table 3), meaning enhanced adhesion properties. Several reasons could be developed to explain this modification. First, this component may increase due to the formation of specific groups such as −(C═O)OH, −CHF, or −FC═O, on the polymer surface. Oxygen plays a key role on this increase; several sources could be involved either during the process or after the reaction when the sample was exposed to air. Some C−H and C−C bonds are broken during the fluorination with F_2 gas and react with oxygen during the transfer in air. Moreover it is important to keep in mind that fluorination processes also modify the roughness of the polymer surface, which is highly increased after direct fluorination treatments. F-LDHs as fluorinating agents seem to avoid, or at least reduce, such side phenomena because a defined amount of atomic fluorine is involved. On the contrary, the gaseous flux results in an excess of F_2 on the surface resulting in higher density of dangling bonds, which react with oxygen, and higher roughness due to hyper-

dx.doi.org/10.1021/ic402193x | Inorg. Chem. 2014, 53, 852−860

fluorination and formation of gaseous CF_4 and C_2F_6 gas (i.e., decomposition in fluorine atmosphere).

CONCLUSION

Layered double hydroxides with controlled Co^{II}/Fe^{III} cations distribution were fluorinated with molecular F_2 gas. The completion of both the conversion from M−OH hydroxide into M−F fluoride and the oxidation of the divalent Co cations seem to be reached at 200 °C. At lowest temperature, that is, 150 °C, an intermediate phase of rutile MF_2-type is suggested by PDF data. The well-ordered arrangement between the metallic ions at the atomic scale is maintained after fluorination thanks to this low reaction temperature (fluorination takes place before decomposition of the LDHs), and a solid solution $Co_{0.60}Fe_{0.40}F_3$ is then prepared. Taking into account that (i) the intimate mixture of Co^{III} and Fe^{III} ions destabilizes each of them in comparison with the single fluorides and finally decreases the decomposition temperature with evolution of atomic fluorine (1 $F^{\bullet}$ per $Co_{0.60}Fe_{0.40}F_3$ unit) and (ii) the possible presence of residual M−OH groups (that reduces the crystallinity of the fluorides and improves the defluorination process), the solid solution of fluorides was used as fluorinating agent for the surface treatment of a commercial polyethylene film, as a representative example of this process. The transfer of fluorine atoms from the fluorinating agent into the polymer has been underlined by both ^{19}F solid state NMR and the change in the surface properties. The present approach of fluorination of LDHs would be extrapolated to other controllable M^{II}/M^{III} mixtures in order to prepare fluorinating agents of different decomposition temperatures. By this method, the fluorination temperature of the target and decomposition of the FA may be fitted on-demand.

ASSOCIATED CONTENT

Supporting Information

Experimental details and characterization data, including XRD and TG, of pure CoF_3 and FeF_3, Rietveld refinement details, and IR spectroscopy of fluorinated LDHs. This material is available free of charge via the Internet at http://pubs.acs.org.

AUTHOR INFORMATION

Corresponding Author

*E-mail: nicolas.louvain@univ-montp2.fr. Tel: +33 467 143 309. Fax: +33 467 143 304.

Present Address

†N.L.: Institut Charles Gerhardt UMR CNRS 5253 (AIME), Université Montpellier 2, CC1502, place E. Bataillon, 34095 Montpellier cedex 5, France.

Author Contributions

The manuscript was written through contributions of all authors. All authors have given approval to the final version of the manuscript.

Notes

The authors declare no competing financial interest.

ACKNOWLEDGMENTS

Pair Diffusion Function measurements done at Argonne and use of the Advanced Photon Source, an Office of Science User Facility operated for the U.S. DOE/Office of Science by Argonne National Laboratory, was supported by the U.S. DOE, Contract No. DE-AC02-06CH11357. K. W. Chapman and D. Dambournet are acknowledged for measuring and extracting the PDF data.

REFERENCES

(1) Hiyama, T. In *Organofluorine Compounds: Chemistry and Applications*; Yamamoto, H., Ed.; Springer-Verlag: New York, 2000.
(2) *Fluorine Chemistry at the Millennium: Fascinated by Fluorine*; Banks, R. E., Ed.; Elsevier Ltd.: New York, 2000.
(3) Touhara, H.; Okino, F. *Carbon* **2000**, *38*, 241−267.
(4) Dukat, W. W.; Holloway, J. H.; Hope, E. G.; Rieland, M.; Townson, P. J.; Powell, R. L. *J. Fluorine Chem.* **1991**, *54*, 221.
(5) Bondalapati, S.; Reddy, U. C.; Kundu, D. S.; Saikia, A. K. *J. Fluorine Chem.* **2010**, *131*, 320−324.
(6) Goryunkov, A. A.; Markov, V. Y.; Boltalina, O. V.; Zemva, B.; Abdul-Sada, A. K.; Taylor, R. *J. Fluorine Chem.* **2001**, *112*, 191−196.
(7) Guérin, K.; Dubois, M.; Houdayer, A.; Hamwi, A. *J. Fluorine Chem.* **2012**, *134*, 8−14.
(8) Zhang, W.; Guérin, K.; Dubois, M.; Fawal, Z. E.; Ivanov, D. A.; Vidal, L.; Hamwi, A. *Carbon* **2008**, *46*, 1010−1016.
(9) Zhang, W.; Guérin, K.; Dubois, M.; Houdayer, A.; Masin, F.; Hamwi, A. *Carbon* **2008**, *46*, 1017−1024.
(10) Batisse, N.; Guérin, K.; Dubois, M.; Hamwi, A.; Spinelle, L.; Tomasella, E. *Thin Solid Films* **2010**, *518*, 6746−6751.
(11) Kharitonov, A. P.; Simbirtseva, G. V.; Bouznik, V. M.; Chepezubov, M. G.; Dubois, M.; Guérin, K.; Hamwi, A.; Kharbache, H.; Masin, F. *J. Polym. Sci., Part A: Polym. Chem.* **2011**, *49*, 3559−3573.
(12) Zhang, W.; Dubois, M.; Guérin, K.; Hamwi, A. *J. Fluorine Chem.* **2007**, *128*, 1402−1409.
(13) Piotrowski, K.; Mondal, K.; Wiltowski, T.; Dydo, P.; Rizeg, G. *Chem. Eng. J.* **2007**, *131*, 73−82.
(14) Leroux, F.; Forano, C.; Prevot, V.; Taviot-Gueho, C. In *Encyclopedia of Nanoscience and Nanotechnology*; Nalwa, H. S., Ed.; American Scientific Publishers: Stevenson Ranch, CA, 2011; Vol. *15*, pp 413−453.
(15) Intissar, M.; Segni, R.; Payen, C.; Besse, J.; Leroux, F. *J. Solid State Chem.* **2002**, *167*, 508−516.
(16) Leroux, F.; Roussel, H.; Flank, A.; Briois, V.; Besse, J. *Clays Clay Miner.* **2002**, *50*, 254−264.
(17) Intissar, M.; Jumas, J.; Besse, J.; Leroux, F. *Chem. Mater.* **2003**, *15*, 4625−4632.
(18) Ma, R.; Liu, Z.; Takada, K.; Iyi, N.; Bando, Y.; Sasaki, T. *J. Am. Chem. Soc.* **2007**, *129*, 5257−5263.
(19) Baird, T.; Campbell, K. C.; Holliman, P. J.; Hoyle, R.; Noble, G.; Stirling, D.; Williams, B. P. *J. Mater. Chem.* **2003**, *13*, 2341−2347.
(20) Leroux, F., Prévot, V., Scott, R. A., Lukehart, C. M., Eds.; *Nanomaterials: Inorganic and Bioinorganic perspectives*; John Wiley & Sons, Ltd: Chichester, UK, 2008; pp 589−618.
(21) Kharitonov, A. P.; Taege, R.; Ferrier, G.; Teplyakov, V. V.; Syrtsova, D. A.; Koops, G. *J. Fluorine Chem.* **2005**, *126*, 251−263.
(22) Chupas, P. J.; Qiu, X.; Hanson, J. C.; Lee, P. L.; Grey, C. P.; Billinge, S. J. *J. Appl. Crystallogr.* **2003**, *36*, 1342−1347.
(23) Chupas, P. J.; Chapman, K. W.; Lee, P. L. *J. Appl. Crystallogr.* **2007**, *40*, 463−470.
(24) Hammersley, A. P. Fit2D Version 9.129 Reference Manual version 3.1, ESRF98HA01T; ERSF Internal report, 1998; pp 1−306.
(25) Qiu, X.; Thompson, J. W.; Billinge, S. J. L. *J. Appl. Crystallogr.* **2004**, *37*, 678−678.
(26) Louvain, N.; Fakhry, A.; Bonnet, P.; El-Ghozzi, M.; Guérin, K.; Sougrati, M.; Jumas, J.; Willmann, P. *CrystEngComm* **2013**, *15*, 3664−3671.
(27) Harris, R. K.; Monti, G. A. In *Solid state NMR of polymers*; Ando, I., Asakura, T., Eds.; Studies in Physical and Theoretical Chemistry; Elsevier: Amsterdam, 1998; Vol. *84*, pp 253−266.
(28) Calleja, G.; Houdayer, A.; Etienne calas, S.; Bourgogne, D.; Flaud, V.; Silly, G.; Shibahara, S.; Takahara, A.; Jourdan, A.; Hamwi, A. *J. Polym. Sci., Part A: Polym. Chem.* **2011**, *49*, 1517−1527.
(29) Varcoe, J. R.; Slade, R. C.; Lam How Yee, E.; Poynton, S. D.; Driscoll, D. J.; Apperley, D. C. *Chem. Mater.* **2007**, *19*, 2686−2693.

(30) Dec, S. F.; Wind, R. A.; Maciel, G. E. *Macromolecules* **1987**, *20*, 2754−2761.
(31) Aimi, K.; Ando, S. *Magn. Reson. Chem.* **2004**, *42*, 577−588.
(32) Owens, D. K.; Wendt, R. C. *J. Appl. Polym. Sci.* **1969**, *13*, 1741−1747.
(33) van Krevelen, D. W.; te Nijenhuis, K. *Properties of Polymers: Their Correlation with Chemical Structure; Their Numerical Estimation and Prediction from Additive Group Contributions*, 4th ed.; Elsevier: New York, 2009.
(34) Kharitonov, A. P. *Prog. Org. Coat.* **2008**, *61*, 192−204.
(35) Kharitonov, A. P. *Direct Fluorination of Polymers*; Nova Science Publishers: New York, 2008.
(36) Kharitonov, A. P. *J. Fluorine Chem.* **2000**, *103*, 123−127.
(37) Kharitonov, A. P.; Loginov, B. A. *Russ J. Gen. Chem.* **2009**, *79*, 635−641.
(38) Carstens, P.; Marais, S. A.; Thompson, C. J. *J. Fluorine Chem.* **2000**, *104*, 97−107.
(39) Jeong, E.; Bae, T.; Yun, S.; Woo, S.; Lee, Y. *Colloids Surf., A* **2011**, *373*, 36−41.
(40) du Toit, F. J.; Sanderson, R. D.; Engelbrecht, W. J.; Wagener, J. B. *J. Fluorine Chem.* **1995**, *74*, 43−48.
(41) Achereiner, F.; Münstedt, H.; Zeiler, T. *J. Phys.: Conf. Ser.* **2008**, *100*, No. 012032.